Supporting Information

Paired Alkaline Electrolyzer with Furfural Oxidation and Hydrogen Evolution over Noble Metal-Free NiFe/Ni and Co/MXene Catalysts

Xiaopeng Liu[a,‡], *Mohammad Albloushi*[a,‡], *Michael Galvin*[a], *Connor W. Schroeder*[a], *Yue Wu*[a,*], *Wenzhen Li*[a,*]

a. Department of Chemical and Biological Engineering, Iowa State University, 618 Bissell Road, Ames, IA 50011, USA

‡ These authors contributed equally to the work.

* Correspondence authors.

Wenzhen Li: E-mail: wzli@iastate.edu; Tel: +1-515-294-4582

Yue Wu: E-mail: yuewu@iastate.edu; Tel: +1-515-294-0702

Equation for Calculation

For OER, all the reported potentials were calibrated with respect to the RHE following the equation:

$$\mathrm{E\,(RHE)} = \mathrm{E}\left(\frac{\mathrm{Ag}}{\mathrm{AgCl}}\right) + 0.0591\mathrm{pH} + 0.196 \quad (1)$$

For HER, all the reported potentials were calibrated with respect to the RHE following the equation:

$$\mathrm{E\,(RHE)} = \mathrm{E}\left(\frac{\mathrm{Hg}}{\mathrm{HgO}}\right) + 0.0591\mathrm{pH} + 0.098 \quad (2)$$

The faradaic efficiency for products was calculated by the equation:

$$\mathrm{FE} = \frac{\mathrm{n} \times \mathrm{z} \times \mathrm{F}}{\mathrm{Q}} \times 100\% \quad (3)$$

In which n is the number of moles of the product, z is the number of electrons required to produce the product, F is the Faraday constant, and Q is the charge released.

The conversion towards 2-furoic acid was calculated by the equation:

$$\mathrm{Conversion}(\%) = \frac{\mathrm{Amount\ of\ furfural\ consumed}}{\mathrm{Initial\ amount\ of\ furfural}} \times 100\% \quad (4)$$

Reaction Mechanism

Anode reaction:

$$C_5H_4O_2 + 3OH^- = C_5H_3O_3^- + 2H_2O + 2e^-$$

Cathode reaction:

$$2H_2O + 2e^- = H_2 + 2OH^-$$

Overall reaction:

$$C_5H_4O_2 + OH^- = C_5H_3O_3^- + H_2$$

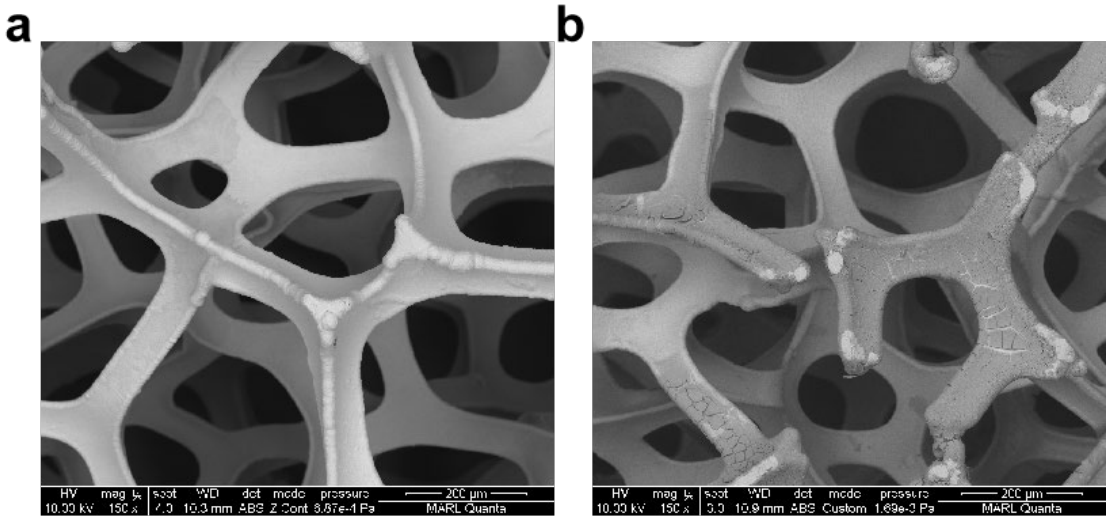

Figure. S1. SEM images of (a) Ni foam and (b) NiFe/NF after electrochemical deposition.

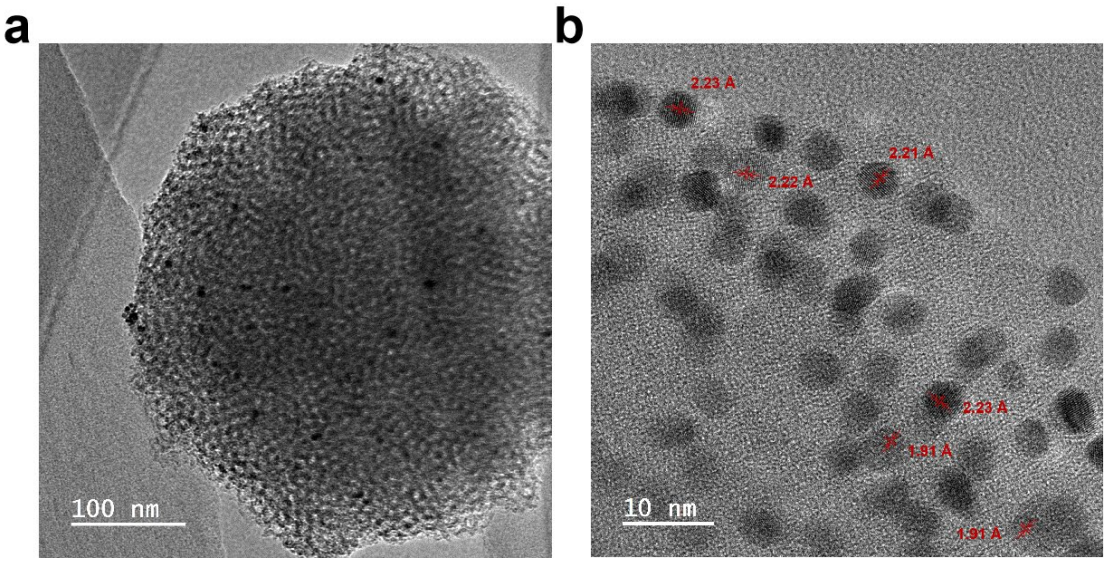

Figure. S2. (a) TEM image of separated spherical composites on the amorphous NiFe nanosheets. (b) Magnified TEM image of the separated sphere showing the alloy nanoparticles.

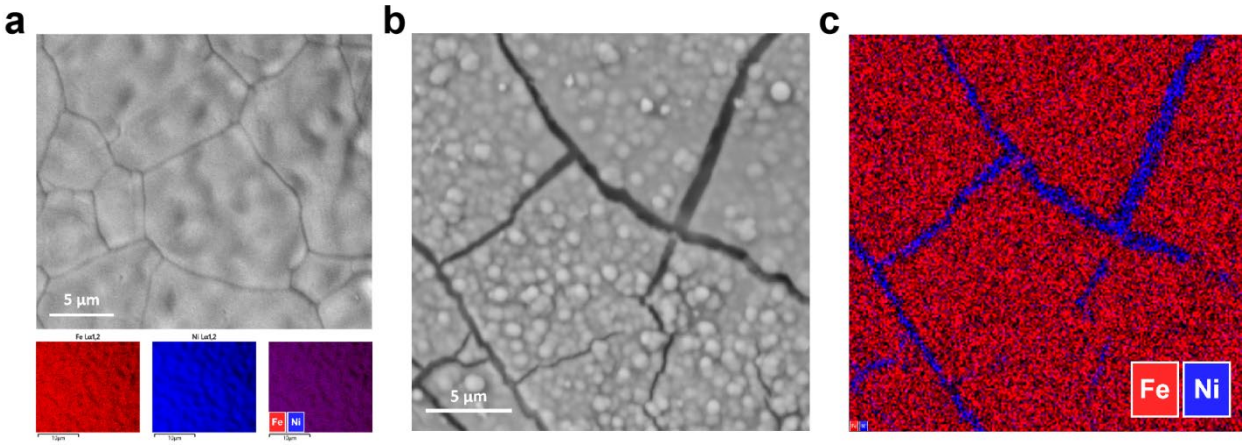

Figure. S3. (a) SEM image of the NiFe/NF catalyst and EDS elemental mappings for Fe and Ni, showing the Fe in red, Ti in blue. (b) SEM image and (c) overlay of Fe and Ni EDS elemental mappings on another area on the NiFe/NF catalyst.

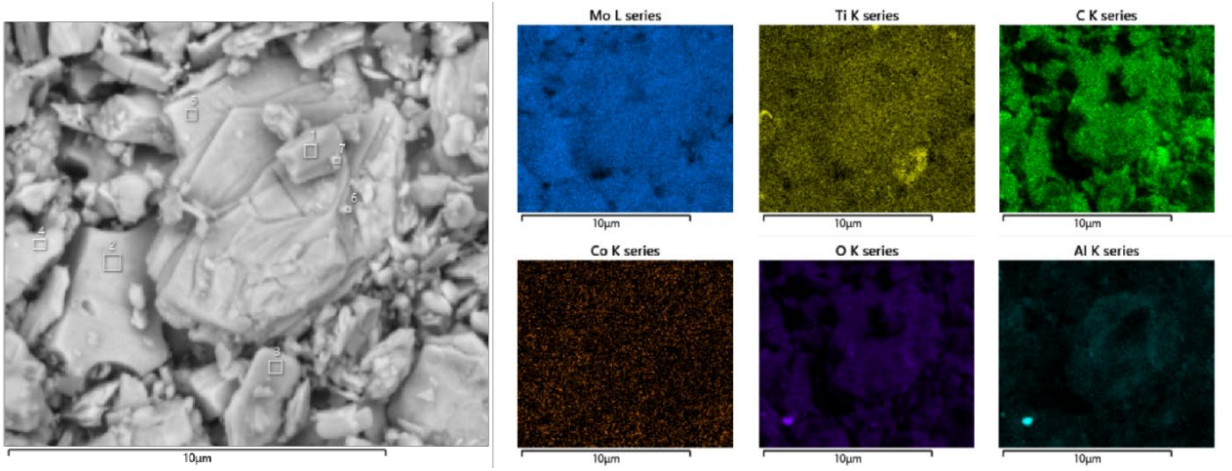

Figure. S4. SEM images of Co/Mo_2TiC_2-700 with EDS elemental mappings for Mo, Ti, C, Al, Co, and O.

Table. S1. Atomic ratio of elements from EDS on selected regions of Co/Mo_2TiC_2-700 catalyst.

Spectrum Label	Mo	Ti	C	Co	Cl	Al	O	Total
Co/Mo_2TiC_2-700 10000x Area1	20.90	9.24	35.67	2.56	0.18	3.13	28.32	100.00
Co/Mo_2TiC_2-700 10000x Area2	35.12	14.53	25.83	6.06	0.17	1.41	16.87	100.00
Co/Mo_2TiC_2-700 10000x Area3	21.23	10.65	34.92	5.08	0.19	1.42	25.50	100.00
Co/Mo_2TiC_2-700 10000x Area4	18.94	10.97	35.67	2.79	0.16	2.31	29.16	100.00
Co/Mo_2TiC_2-700 10000x Area5	19.15	10.63	33.60	3.00	0.09	2.68	30.86	100.00
Co/Mo_2TiC_2-700 10000x Area6	16.34	8.24	35.39	3.34	0.04	4.39	32.26	100.00
Co/Mo_2TiC_2-700 10000x Area7	17.67	7.88	35.00	2.15	0.07	3.55	33.67	100.00

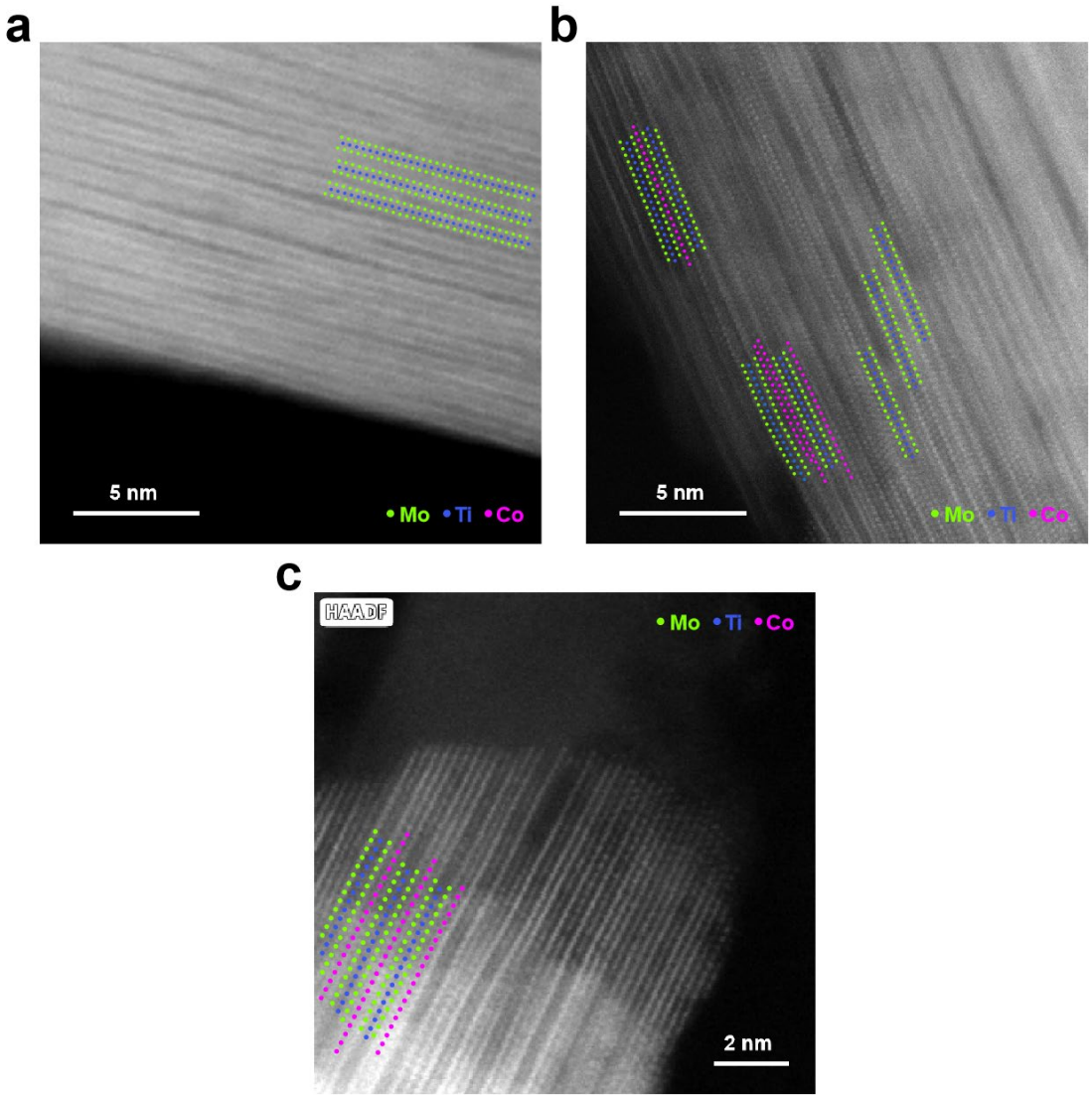

Figure. S5. TEM showing the Co distribution on (a) Co/Mo_2TiC_2-500, (b) Co/Mo_2TiC_2-600, and (c) Co/Mo_2TiC_2-700 catalysts.

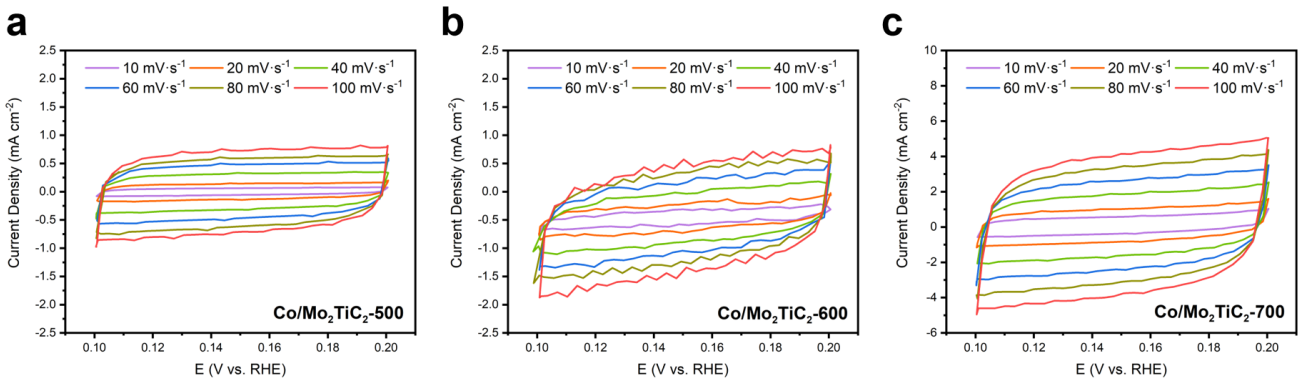

Figure. S6. Cyclic voltammetry (CV) curves of (a) Co/Mo_2TiC_2-500, (b) Co/Mo_2TiC_2-600, and (c) Co/Mo_2TiC_2-700 at different scan rates in a non-faradaic region.

Table. S2. Summary of high current density overpotential catalyzed by Co/Mo_2TiC_2 catalysts and Pt in H-cell.

Samples	Mass of active metal (Co or Pt)	Overpotential @ 100 mA/cm^2	Overpotential @ 200 mA/cm^2	Overpotential @ 300 mA/cm^2	Overpotential @ 400 mA/cm^2
Co/Mo_2TiC_2-700	0.50 mg/cm^2	244 mV	276 mV	299 mV	321 mV
Co/Mo_2TiC_2-600	0.49 mg/cm^2	274 mV	333 mV	369 mV	394 mV
Co/Mo_2TiC_2-500	0.51 mg/cm^2	306 mV	373 mV	433 mV	474 mV
Commercial 40% Pt/C	0.57 mg/cm^2	216 mV	280 mV	326 mV	365 mV

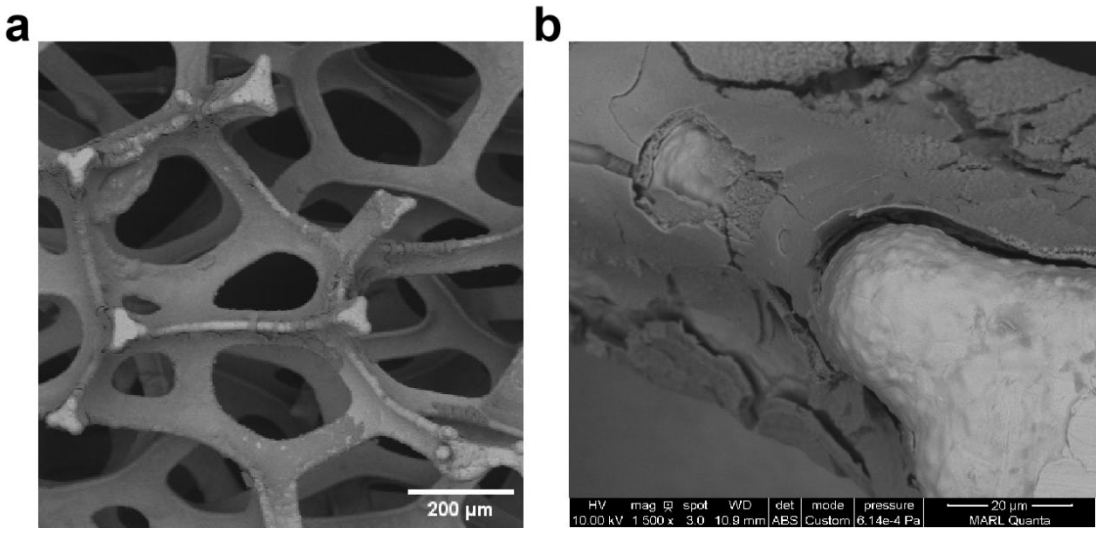

Figure. S7. SEM of the NiFe/NF anode after the flow cell test.

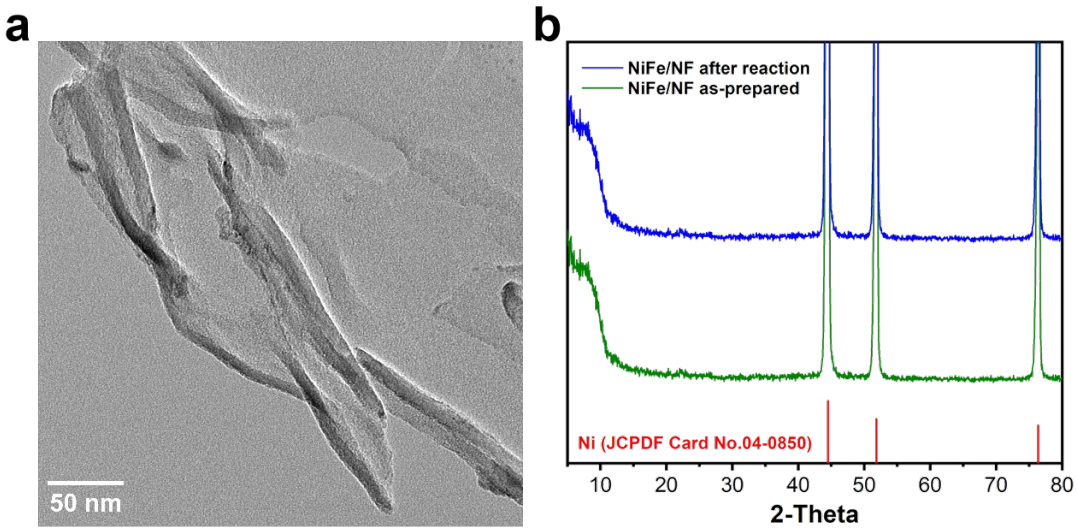

Figure. S8. (a) TEM image of the NiFe nanosheets scratched off from the NiFe/NF anode after the electrochemical test, (b) XRD patterns of NiFe/NF samples before and after the electrochemical reaction, the red vertical lines are the standard XRD pattern of nickel (JCPDF Card No. 04-0850).

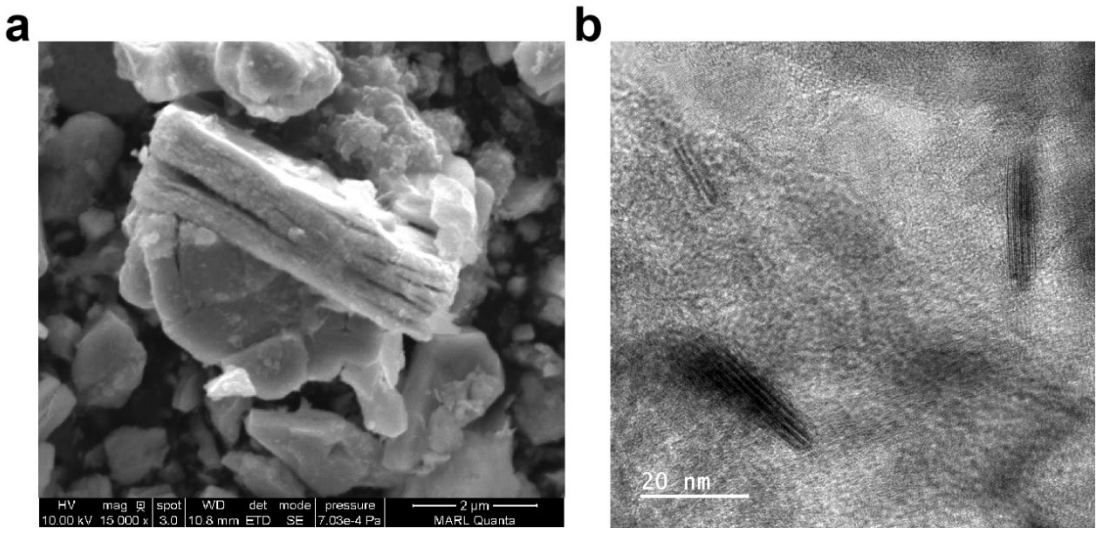

Figure. S9. (a) SEM and (b) TEM of the Co/Mo_2TiC_2-700 scraped off the cathode after the flow cell test.

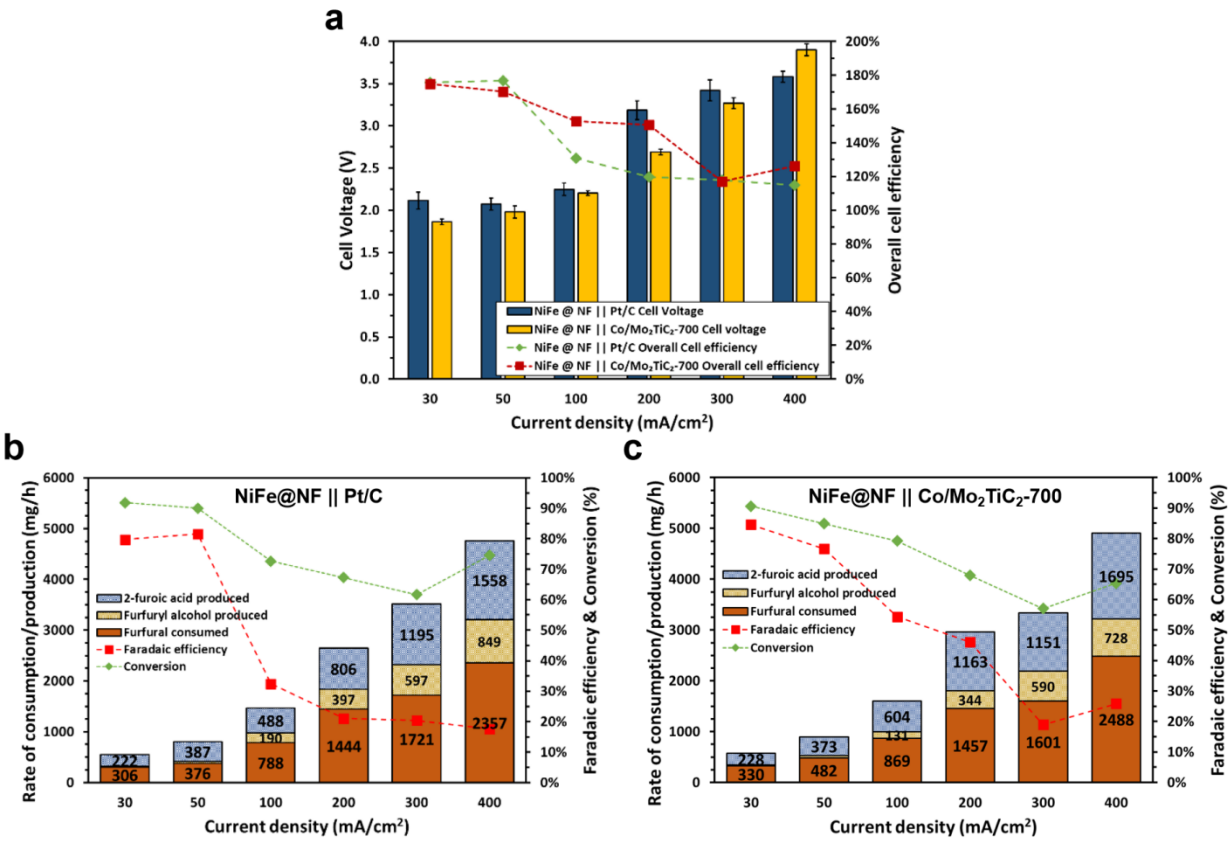

Figure. S10. (a) The flow cell performance (Cell voltage and Faradaic efficiency) over 3 hours of electrolysis, and (b, c) the anode performance (Rate of consumption/production and Faradaic efficiency & Conversion) to compare the Co/Mo_2TiC_2-700 and Pt/C catalysts at 30 - 400 mA/cm^2.

To acquire deep understanding of the FOR/HER paired electrolyzer, a thermodynamic analysis was carried out to deallocate the cell voltage observed at high current densities (50 mA/cm² – 200 mA/cm²). The commencement of such analysis involves using the data of the half electrochemical reactions obtained in the H-type cell. The thermodynamic properties of furfural oxidation to 2-furoic acid, represented by Equation 5, were delineated. Equation 6 shows the hydrogen evolution reaction. The summation of these reactions yields the overall redox reaction, which manifests the cell's thermodynamic potential and discerns its classification as either Galvanic or electrolytic. In accordance with Equation 7, an electrolytic cell signifies a reaction requiring external energy input for propulsion (an electrolyzer). To qualify as a galvanic cell, the cell's thermodynamic potential must surpass zero.

$$C_5H_4O_2 + 2OH^- \longrightarrow C_5H_4O_3 + H_2O + 2e^-,\ E^o_{RHE} = 0.068\,V \tag{5}$$

$$2H_2O + 2e^- \longrightarrow 2OH^- + H_2\,,\ E^o_{RHE} = 0\,V \tag{6}$$

$$C_5H_4O_2 + H_2O \longrightarrow C_5H_4O_3 + H_2\,,\ E^o_{cell} = -0.068\,V \tag{7}$$

Acquiring this information is pivotal for elucidating the constituent overpotentials that contribute to the comprehensive overall cell voltage. To accomplish this, the calculated cell voltage, as presented in Equation 8 [10], serves as a means of comparison against the experimentally measured cell voltage. Equation 8 encapsulates both cathodic and anodic overpotentials, the determination of which can be facilitated through the utilization of Equation 9. The assessment of ohmic drop, on the other hand, is fundamentally conducted through the application of Ohm's law, wherein V represents voltage, I denotes current, and R signifies resistance.

$$V_{Cell} = U_{Cell} - |\eta_{s,anode}| - |\eta_{s,cathode}| - |\eta_{conc,anode}| - |\eta_{conc,cathode}| - |\eta_{ohmic}| \tag{8}$$

Where:

- V_{Cell} is the calculated cell voltage (V).
- U_{Cell} is the thermodynamic potential of the redox reaction (V).
- $\eta_{s,anode}$ is the anodic overpotential (V).
- $\eta_{s,cathode}$ is the cathodic overpotential (V).
- $\eta_{conc,anode}$ is the anolyte concentration overpotential (V).
- $\eta_{conc,cathode}$ is the catholyte concentration overpotential (V).
- η_{ohmic} is ohmic drop or internal resistance induced overpotential (V).

$$\eta_{s,i} = E^o - E \quad (9)$$

Where:

- $\eta_{s,i}$ is the anodic or cathodic overpotential (V).
- E^o is the standard potential of the half-cell reaction in the cathode (V).
- E is the applied potential during the experiment (V).

Utilizing the introduced mathematical expressions, an analysis was conducted on current densities ranging from 50 mA/cm² to 200 mA/cm², aiming to compare the computed cell voltage with the experimentally measured counterpart obtained by the electrochemical workstation. Discrepancies between the calculated and measured cell voltages are detailed in Tables S3 and S4. It is interesting to find that the differences between measured and calculated cell voltages are 0.22~0.55 V, this may be attributed to 1) the omission of anolyte and catholyte overpotentials in the analytical framework, and 2) direct use of the anodic/cathodic potentials obtained from the half-cell tests. Nevertheless, upon a comparative examination of the two voltage datasets, a consistent observation emerges: the calculated cell voltage consistently registers as lower than the measured voltage. This actually provides us with a useful tool to analyze the distribution of overpotentials from anodic and cathodic kinetics, and internal resistance (Ohmic loss), thus guiding future design of more efficient flow cells. It should be noted that anolyte and catholyte overpotentials were not included (estimated) in the analytical considerations.

Table. S3. NiFe/NF || Pt/C electrolyzer cell voltage comparison between calculated and measured. Note: anodic and cathodic potentials were measured in half-cell tests.

resistance (ohms)	Current Density (mA/cm^2)	Anodic potential (V vs. RHE)	Cathodic potential (V vs. RHE)	$\eta_{s,anode}$	$\eta_{s,cathode}$	η_{ohmic}	$V_{cell,\ calculated}$	$V_{cell,\ measured}$
0.858	50	1.488	-0.280	1.371	0.163	0.172	1.774	1.951
1.48	100	1.51	-0.326	1.388	0.216	0.592	2.264	2.249
1.07	200	1.521	-0.365	1.420	0.280	0.856	2.623	3.185

Table. S4. NiFe/NF || Co/Mo_2TiC_2-700 electrolyzer cell voltage comparison between calculated and measured. Note: anodic and cathodic potentials were measured in half-cell tests.

resistance (ohms)	Current Density (mA/cm^2)	Anodic potential (V vs. RHE)	Cathodic potential (V vs. RHE)	$\eta_{s,anode}$	$\eta_{s,cathode}$	η_{ohmic}	$V_{cell,\ calculated}$	$V_{cell,\ measured}$
0.684	50	1.488	-0.215	1.371	0.214	0.137	1.790	1.979
0.684	100	1.510	-0.244	1.388	0.244	0.274	1.973	2.204
0.874	200	1.521	-0.276	1.420	0.276	0.6992	2.463	2.688

Table. S5. Comparison of state-of-the-art ECO-HER electrolyzers reported in the literature.

Anodic Catalyst	Anolyte	Cathodic Catalyst	Catholyte	Current density (mA/cm^2)	Cell voltage (V)	Anodic Faradaic efficiency (%)	Cathodic Faradaic efficiency (%)	Reference
Co-P/CF	1 M KOH + 50 mM HMF	Co-P/CF	1 M KOH	20	1.38	93%	100%	[1]
Ni_2P/NF	1 M KOH + 10 mM HMF	Ni_2P/NF	1 M KOH	50	1.58	98%	100%	[2]
hp-Ni/NF	1 M KOH + 10 mM HMF	hp-Ni/NF	1 M KOH	100	1.66	97%	100%	[3]
Ni_3N/C	1 M KOH + 10 mM HMF	Ni3N@C	1 M KOH	50	1.55	100%	-	[4]
$Cu_xS/Ni_{0.75}Co_{0.25}O_mH_n$	1 M KOH + 10 mM HMF	$Cu_xS/Ni_{0.75}Co_{0.25}O_mH_n$	1 M KOH	100	1.58	100%	100%	[5]
Ni_3S_2/NF	1 M KOH + 10 mM HMF	Ni_3S_2/NF	1 M KOH	100	1.64	98%	100%	[6]
Ni_2P/Ni/NF	1 M KOH + 30 mM furfural	NiP/Ni/NF	1 M KOH	175	1.6	98%	100%	[7]
$Ni_2Fe(CN)_6$	0.33 M Urea + 1 M KOH	RuO_2	1 M KOH	100	1.35	-	90%	[8]
Ni-NiO	0.5 M Urea + 1 M KOH	Ni-NiO	1 M KOH	10	1.475	-	-	[9]
NiFe/NF	1 M KOH + 100 mM furfural	Co/Mo_2TiC_2-700	1 M KOH	400	3.899	50% (65% conversion)	100%	This work

References

[1] N. Jiang, B. You, R. Boonstra, I. M. Terrero Rodriguez and Y. Sun, *ACS Energy Lett.*, 2016, **1**, 386-390.

[2] B. You, N. Jiang, X. Liu and Y. Sun, *Angew. Chem. Int. Ed.*, 2016, **55**, 9913-9917.

[3] B. You, X. Liu, X. Liu, and Y. Sun, *ACS Catal.*, 2017, **7**, 4564-4570.

[4] N. Zhang, Y. Zou, L. Tao, W. Chen, L. Zhou, Z. Liu, B. Zhou, G. Huang, H. Lin and S. Wang, *Angew. Chem. Int. Ed.*, 2019, **58**, 15895-15903.

[5] X. Deng, X. Kang, M. Li, K. Xiang, C. Wang, Z. Guo, J. Zhang, X.Z. Fu and J. L. Luo, *J. Mater. Chem. A*, 2020, **8**, 1138-1146.

[6] B. You, X. Liu, N. Jiang and Y. Sun, *J. Am. Chem. Soc.*, 2016, **138**, 13639-13646.

[7] N. Jiang, X. Liu, J. Dong, B. You, X. Liu, Y. Sun, *ChemNanoMat*, 2017, **3**, 491-495.

[8] S. K. Geng, Y. Zheng, S. Q. Li, H. Su, X. Zhao, J. Hu, H. B. Shu, M. Jaroniec, P. Chen, Q. H. Liu and S. Z. Qiao, *Nat. Energy*, 2021, **6**, 904-912.

[9] X. Xu, X. Hou, P. Du, C. Zhang, S. Zhang, H. Wang, A. Toghan and M. Huang, *Nano Res*., 2022, **15**, 7124-7133.